CrossMark

The influence of Ag substitution on structural and mechanical properties of (Bi, Pb)-2223 ceramics

Burcu Cevizci[1] · Ozlem Bilgili[1] · Kemal Kocabaş[1]

Abstract In this work, $Bi_{1.7}Pb_{0.3}Sr_2Ca_2Cu_{3-x}Ag_xO_y$ (x = 0.00, 0.03, 0.06, 0.09, 0.12) ceramics were prepared by conventional solid state reaction method. The effects of Ag substitution on the structural and mechanical properties of the samples were investigated by Vickers microhardness, X-ray powder diffraction (XRD) measurements and scanning electron microscope (SEM) analysis. The phase formation, volume fraction and lattice parameters were characterized by using XRD measurements. Surface morphology and grain connectivity of the samples were identified by using SEM. The mechanical properties were analyzed by microhardness measurements. Load dependent microhardness, elastic modulus, yield strength and fracture toughness were obtained by hardness measurements. XRD results indicated that the lattice parameter c decreases with increasing Ag addition. It was also observed that volume fraction of Bi-2223 phase decreases with increasing Ag addition from XRD measurements. SEM results showed that the surface morphology and grain connectivity improve, the grain sizes and porosity of the samples decrease with increasing Ag addition. Vickers microhardness (H_v), Young's modulus (E), yield strength (Y) and fracture toughness (K_{IC}) values were calculated separately for all samples. In our study, Young's modulus, yield strength, and fracture toughness of the samples indicated dependency on applied load. It was seen that the load dependent H_v, E, Y, and K_{IC} increase with increasing Ag and decreasing applied load. Experimental results of the microhardness measurements were analyzed using two models such as elastic–plastic deformation model and the energy dissipative model. Energy dissipative model was determined as the most successful model describing the mechanical properties of our samples.

1 Introduction

Since the discovery of superconductivity, researchers have studied to improve the superconducting, mechanical and structural properties of the superconducting materials. It is known that preparation method, chemical doping, addition, substitution, annealing time and temperature play a very important role in cuprate superconducting systems. The effect of addition of various elements and annealing process on the superconducting and mechanical properties of Bi-2223 high temperature superconductors are studied in literature [1–19].

Due to structure of Bi-2223 superconductors, these compounds have high brittleness and low ductility resulting limited usage of these materials. Improving mechanical properties of this material without affecting superconductivity or critical current carrying capacity is difficult due to poor mechanical properties of Bi-2223. On the other hand, Bi-2223 superconductors have plate-like grains which are easier to texture during processing [20]. The improvement of mechanical properties such as hardness, elastic modulus, yield strength, fracture toughness of superconductor ceramics are very critical for their use in industrial applications.

In order to determine mechanical properties of materials, various methods such as bending test, compression test and microhardness test etc. were used. The Vickers microhardness indention testing is a useful tool to probe the mechanical properties of brittle materials as superconductors. This test is one of the most convenient methods to estimate the

✉ Ozlem Bilgili
  ozlem.bilgili@deu.edu.tr

[1] Department of Physics, Faculty of Science, Dokuz Eylül University, Izmir, Turkey

mechanical properties, the relationship between Vickers hardness, elastic modulus, yield strength and fracture toughness for polycrystalline superconductors at room temperature [9, 21–23].

In this study, the effects of Ag substitution for Cu in $Bi_{1.7}Pb_{0.3}Sr_2Ca_2Cu_{3-x}Ag_xO_y$ (x = 0.00, 0.03, 0.06, 0.09, 0.12) on structural and mechanical properties of Bi-2223 ceramics have been investigated. The purpose of this study is to examine the load dependence of apparent hardness, determine load independent hardness values of the samples and investigate true hardness values with two different models. Vickers microhardness measurements were done to analyze the mechanical properties of samples. Scanning electron microscopy (SEM) and X-Ray Diffraction (XRD) were done to investigate the surface microstructure of the samples, crystal structure and lattice parameters determination.

2 Experimental details

$Bi_{1.7}Pb_{0.3}Sr_2Ca_2Cu_{3-x}Ag_xO_y$ (x = 0.00, 0.03, 0.06, 0.09, 0.12) ceramic superconducting system was synthesized by using solid state reaction method. Bi_2O_3, PbO, SrCO, $CaCO_3$, CuO and Ag_2O with high purity (%99.99) was used. Samples with different substitution ratios of Cu by Ag_2O have been prepared and labelled Ag0 (x = 0.00), Ag1 (x = 0.03), Ag2 (x = 0.06), Ag3 (x = 0.09), and Ag4 (x = 0.12). The powders were throughly mixed and grounded. After milling, the mixed powders were calcined at 800 °C for 20 h in alumina crucibles in air. After this process, the samples cooled to room temperature. The calcined powders were grounded again and pressed at 450 MPa pressure. Prepared pellets were 13 mm in diameter and have 1–1.5 mm thickness. These pellets were further sintered at 845 °C for 100 h. After sintering, the pellets were furnace-cooled down to room temperature.

X-ray diffraction studies were performed for the phase identification of our samples. Diffraction patterns were obtained by utilizing CuK_α radiation with a wavelength λ of 1.5418 A°. XRD measurements were scanned for a wide range of diffraction angles (2θ) ranging from 3° to 60°. The phase purity, the lattice parameters and crystal structure of samples were obtained from XRD patterns. The volume fractions of the Bi-2223 and Bi-2212 phases were determined from the peak intensities of H(hkl) and L(hkl) reflections, using the following well-known expressions [24].

$$Bi\text{-}(2223)\% = \frac{\sum I(2223)}{\sum I(2223) + \sum I(2212)} \times 100 \quad (1)$$

$$Bi\text{-}(2212)\% = \frac{\sum I(2212)}{\sum I(2223) + \sum I(2212)} \times 100 \quad (2)$$

Here $\sum I(2223)$ and $\sum I(2212)$ are the intensities of the (hkl) diffraction lines for Bi-2223 and Bi-2212 phases, respectively.

Grain size of the samples can be determined from XRD patterns using Scherrer Formula which is shown in Eq. (3) [19, 25–27].

$$D = \frac{0.9\lambda}{B\cos\theta} \quad (3)$$

Here D is the mean size of grain. λ is the X-ray wavelength, B is the line broadening at half the maximum intensity (FWHM) in radians, and θ is the Bragg angle. The dimensionless shape factor varies with the actual shape of the crystallite. With using this equation, particles size can be estimated.

The surface morphologies of pure and Ag doped samples were examined by using scanning electron microscope (SEM). The microstructures of the top surfaces of all samples are shown in SEM microphotographs taken at (×2000) magnification.

Hardness measurements of samples were performed by using a digital microhardness tester at room temperature. With a single loading time of 10 s a Vickers pyramidal indenter, five different loads (0.294, 0.490, 0.980, 1.961, and 2.940 N) were applied to samples' surfaces. The diagonal lengths of indentation impressions were measured with an accuracy of ±0.1 μm. Indentations were pressed on the different parts of the samples' surfaces. The distance between any two indentations was more than two times the diagonal of the indentation mark avoiding overlap and surface effects due to neighbouring indentation. An average of five readings at different locations of specimen surfaces was taken to obtain mean values for each load. Vickers microhardness values were calculated and various hardness models were analyzed. Conventional Vickers microhardness measurements consist of applying a load F on the test material via a geometrically defined indenter. Vickers microhardness values were calculated using the following equation [12, 28].

$$H_v = 1854.4\left(\frac{F}{d^2}\right)(GPa) \quad (4)$$

where F is the load applied (N) and d the mean diagonal length of the indentation impression (μm).

3 Results and discussion

3.1 XRD characterization

Figure 1 shows X-ray diffraction patterns of samples Ag0, Ag1, Ag2, Ag3 and Ag4. Characteristic peaks

corresponding to different phases were labelled with different symbols which are filled circle, open circle, diamond, asterisk and indicate the peaks due to the Bi-2223 phase, Bi-2212 phase, and Ca_2PbO_4, CuO impurities phases, respectively. XRD analyses showed two main phases: high-T_c phase (Bi-2223), low-T_c phase (Bi-2212) with some impurities phases like CuO, Ca_2PbO_4.

The characteristic peaks of Bi-2223 system H(002) and L(002) peaks were seen at $2\theta = 4.80°$ and $2\theta = 5.76°$, respectively. The highest intensity value of L(002) peak and H(002) peak was seen at Ag0 sample. H(002) peak has disappeared with increasing addition. Formation of CuO with characteristic diffraction peak at $2\theta = 38.8°$ was seen in undoped sample. CuO peaks disappear in Ag doped samples. Ca_2PbO_4 phase appears at $2\theta = 17.32°$ in all samples. In this study, all peaks of Bi-2223 and Bi-2212 phases have been used for the estimation of the volume fraction of the phases. The volume fractions of Bi-2223 and Bi-2212 phases were calculated from all peak intensities of Bi-2223 and Bi-2212 using Eqs. (1) and (2). The volume fraction of the phases for all samples is given in Table 1. As seen in the table, volume fraction of Bi-2223 phase decrease and volume fraction of Bi-2212 phase increase with increasing substitution of Ag. Volume fraction of low-T_c phase Bi-2212 is the lowest (~ 48 %), corresponding to the highest volume fraction of the high-T_c phase Bi-2223 (~ 52 %) in the Ag0 sample. The lattice parameters (a, b, c) are calculated from Miller indices (hkl) and interplanar distances (d_{hkl}) by least squares method for all samples. The lattice parameters (a, b, c) of the samples are given in Table 1. The crystal system of undoped sample was found to be orthorhombic with the lattice parameters a = 5.399 Å, b = 5.413 Å and c = 37.130 Å. With increasing Ag

substitution, the lattice parameter a remains unchanged, the lattice parameter c decreases gradually. Grain sizes of the samples can be calculated by using the full width at half maximum (FWHM) of the peaks and the Eq. (3). The particle sizes calculated by using Scherrer formula are found as 35.4, 35.7, 36.9, 37.4, and 43.9 nm for Ag0, Ag1, Ag2, Ag3, and Ag4, respectively. The calculated grain sizes are tabulated in Table 1. As can be seen from the table, the grain sizes increase with Ag substitution which is in line with SEM results.

3.2 SEM analyses

Figure 2a–e shows the surface SEM images of the Ag0, Ag1, Ag2, Ag3 and Ag4 samples. It was observed that the microstructures of all samples exhibit a common feature of plate-like grains and are randomly distributed. The grain size of doped samples is larger than the undoped sample, it is also seen that doped samples have denser surface structure. These surface structures are compatible with the microhardness results. As shown in Fig. 2, Ag-substituted sample has less porosity than the undoped sample. Smaller values of hardness are obtained where porosity is high. The results of the hardness values are consistent with SEM results.

Superconducting grains are seen to be connected with each other poorly and the surface morphology of the sample comprises of platelets and layered grains with uniform and homogenous microstructure in the undoped sample. The undoped sample consists of plate-like grains as shown in Fig. 2a. It is also seen that there are some voids along the grain boundaries from the figure. This may be attributed that grains of the undoped sample are poorly connected. The plate-like features are also found in Ag doped samples but the size of the grains are larger than the undoped sample. Microstructural examination revealed that both the number and size of the voids decrease with increasing Ag substitution which may lead to increasing grain connectivity in the sample. The decrease of porosity might be related to increase in grain coupling strength and degree of grain orientation of the BSCCO samples. Bi-2212 phase has higher crystallographic density and stronger intergranular links than Bi-2223 phase. If the XRD patterns of the sample is reexamined, it is seen that Ag4 sample mostly consists of Bi-2212 phase. Therefore, the highest density value would be expected for Ag4 sample.

3.3 Mechanical measurements

To specify the effect of Ag substitution on mechanical properties of samples, the Vickers microhardness values of different applied loads (0.294, 0.490, 0.980, 1.961 and 2.940 N) were calculated. The load dependent (Vickers)
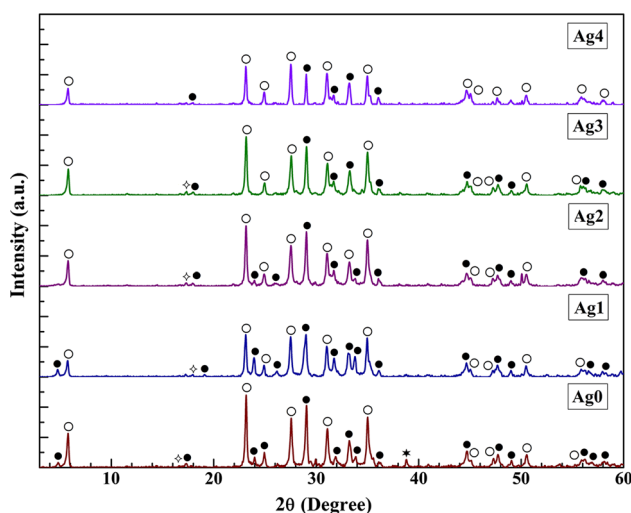

Fig. 1 XRD patterns of the $Bi_{1.7}Pb_{0.3}Sr_2Ca_2Cu_{3−x}Ag_xO_y$ (x = 0.00, 0.03, 0.06, 0.09, 0.12) samples; *filled circle* Bi-2223 phase, *open circle* Bi-2212 phase, *diamond* Ca_2PbO_4, *asterisk* Ca_2PbO_4

Table 1 Lattice parameters (a, b, c), volume fractions of Bi-2223, Bi-2212 phases and grain size for samples Ag0, Ag1, Ag2, Ag3 and Ag4

Sample	a (Å)	b (Å)	c (Å)	Volume fraction (%) Bi-2223	Volume fraction (%) Bi-2212	Grain size (nm)
Ag0	5.399	5.413	37.130	52.40	47.60	35.4
Ag1	5.408	5.421	37.075	49.89	50.11	35.7
Ag2	5.389	5.408	30.550	39.29	60.71	36.9
Ag3	5.395	5.389	30.649	36.60	63.40	37.4
Ag4	5.407	5.412	30.771	25.19	74.81	43.9

microhardness (H_v) can be calculated according to the following equation:

$$H_v = 1854.4 (F/d^2) \ \ (GPa)$$

where F is the applied load in N and d is the diagonal length of the indentation in μm. From the microhardness measurement results, it is observed that the load dependent microhardness values decrease with applied load for all samples as shown in Fig. 3. The variation of load dependent microhardness has a similar shape for all samples. Ag4 sample has the highest microhardness values for all values of applied load. With increasing amount of doping level the microhardness values increase monotonically. The increase of microhardness with doping can be explained by the formation of impurities and the decrease in porosity as observed in SEM measurements.

The measured indentation diagonal lengths and calculated microhardness values of different applied loads are given in Table 2 for each sample. It can be seen from the table that apparent hardness values are load dependent for all samples. The value of H_v is found to vary from 0.425 to 0.224 GPa in the load range of 0.294–2.942 N for Ag0 sample. The corresponding hardness values of the same applied load range are calculated in the range of 0.506–0.248, 0.680–0.278, 0.787–0.314 and 0.894–0.345 GPa for Ag1, Ag2, Ag3 and Ag4, respectively. The change of hardness values with the applied load is depicted in Fig. 3. The curves in the graph show that microhardness values decrease non-linearly as the applied load increased. As can be seen from the graph, hardness values decreased with increasing the applied load to 0.294 N from 2.942 N. This means that the material shows Indentation Size Effect (ISE) behavior that is, hardness decreases with increasing applied load [29–31].

The Young modulus (E) of superconductors is related to the Vickers microhardness by the relation below;

$$E = 81.9635 \, H_v \tag{5}$$

The yield strength (Y) is related to the hardness by the relation [11, 32].

$$Y \approx H_V / 3 \tag{6}$$

The load dependent elastic modulus (E) and the yield strength (Y) values of material are calculated and presented

in Table 2. It is observed that E and Y values decrease with increasing applied load and increase significantly with increasing Ag substitution. The fracture toughness, K_{1C}, is one of the main mechanical properties of superconducting samples and is an important parameter for the selection of materials for applications.

$$K_{IC} = \sqrt{2E\gamma} \tag{7}$$

where E is the load dependent Young's modulus and γ is surface energy. The values of load dependent fracture toughness (K_{1C}) are summarized in Table 2. From this table, it is observed that K_{1C} increases significantly with increasing Ag substitution. The hardness values in plateau region $H_v = 0.239$–0.224 GPa for Ag0, $H_v = 0.270$–0.248 GPa for Ag1, $H_v = 0.298$–0.278 GPa for Ag2, $H_v = 0.332$–0.314 GPa for Ag3, $H_v = 0.371$–0.345 GPa for Ag4 (Figs. 4, 5, 6).

In order to describe the ISE behaviour of materials, several models for the relationship between applied indentation test load and indentation diagonal length have been suggested in the literature [33, 34]. In our study, we have investigated this effect by using two different methods. Both models participate in the determination of the true hardness values of samples.

The first model assumes that the indentation contains an elastic portion. The elastic part of the deformation is relaxed upon loading. This can be accounted for adding an elastic component, d_e, to the measured plastic indentation semidiagonal, d_p. Thus, a true hardness, H_0, is defined from Eq. (8) [35].

$$H_0 = 1854.4 \frac{F}{(d_p + d_e)^2} \tag{8}$$

Therefore, above equation indicates that measured indentation diagonals should be linear with the square root of the applied load and the slope of such a curve (Fig. 7) is proportional to $(H_0)^{1/2}$ and the horizontal intercept of this graph is proportional to the elastic part of the indentation semidiagonal, d_e. It was obvious that such plots are linear with the estimated linear regression coefficients (LRC) always better than 99.7 %, implying that Eq. (8) provides a satisfactory description to calculate the true hardness of the indentation data for the samples. The extracted values of H_0,
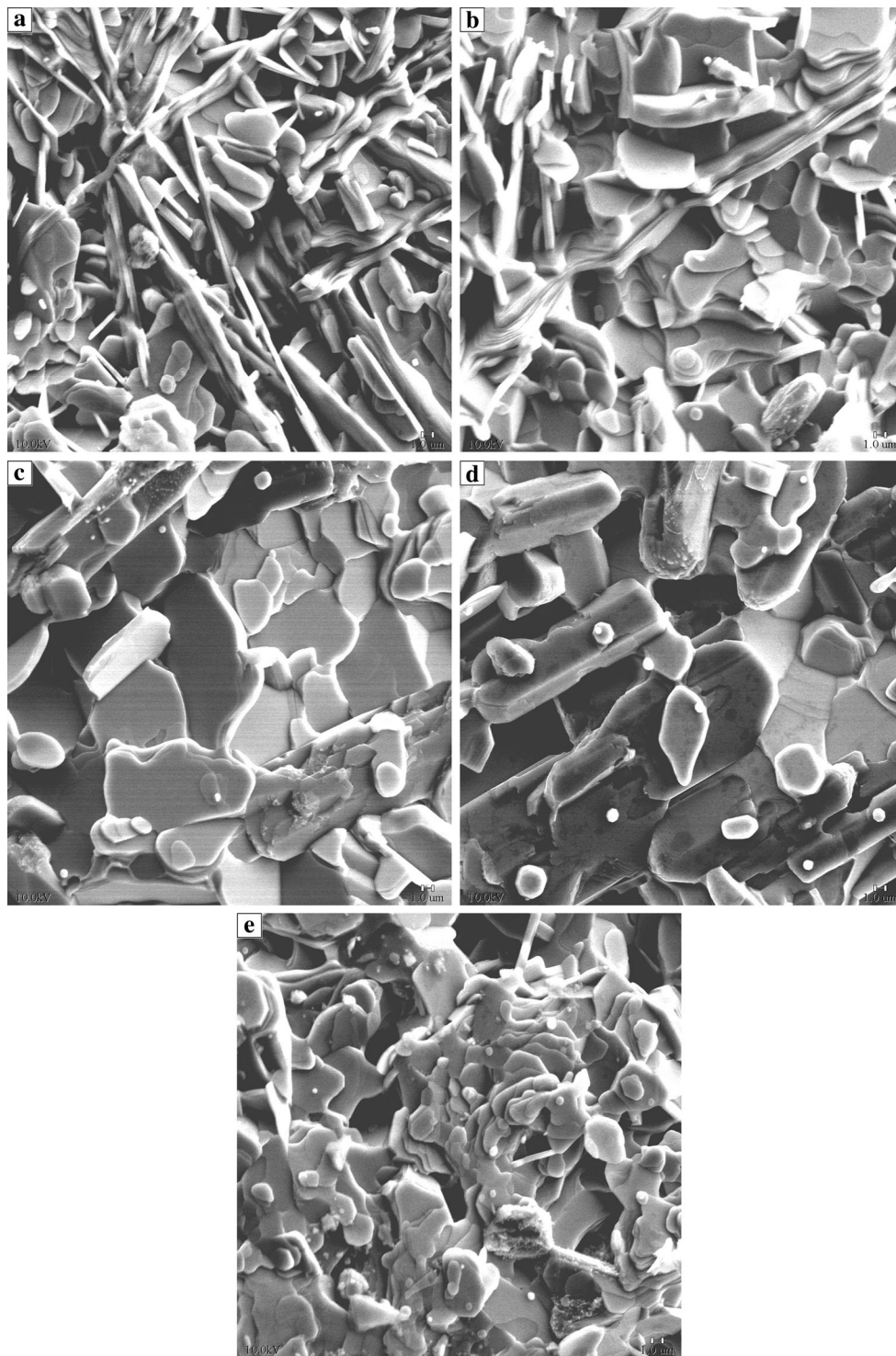
Fig. 2 SEM micrographs of **a** Ag0, **b** Ag1, **c** Ag2, **d** Ag3 and **e** Ag4 samples

d_e and LRC are listed in Table 3. As seen from the table, H_0 values of the samples are found to increase with increasing Ag substitution. If d_e value is negative, elastic deformation is not observed in the material, there is only plastic deformation. d_e values showed negative values indicating plastic deformation. The true microhardness value of Ag0 sample (0.177 GPa) is lower than the hardness results (see Table 3) in the plateau region (saturated region) ($H_v = 0.239$ and 0.224 GPa). This behaviour is observed in other samples (Ag1, Ag2, Ag3 and Ag4) in this work. This result indicates that the true hardness of the sample is lower than that of the traditionally calculated in plateau regions. Although the
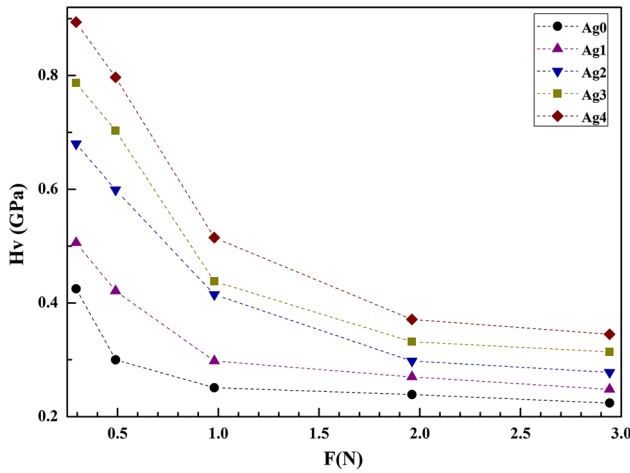
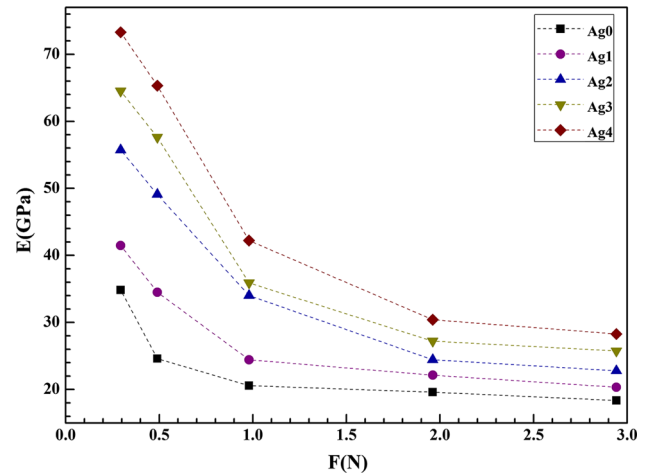**Fig. 3** Variation of microhardness as a function of applied load for Ag0, Ag1, Ag2, Ag3, Ag4 samples

Fig. 4 Variation of Young's modulus as a function of applied load

Table 2 The calculated load dependent H_v, E, Y and K_{IC} for the samples

| Force (N)	H_v (GPa)	E (GPa)	Y (GPa)	K_{IC} (Pa/m$^{1/2}$)
Ag0				
0.294	0.425	34.83	0.142	547.94
0.490	0.300	24.59	0.100	460.40
0.980	0.251	20.57	0.084	421.09
1.961	0.239	19.59	0.080	410.93
2.942	0.224	18.36	0.075	397.82
Ag1				
0.294	0.506	41.47	0.169	715.94
0.490	0.421	34.51	0.140	653.10
0.980	0.298	24.43	0.099	549.50
1.961	0.270	22.13	0.090	522.99
2.942	0.248	20.33	0.083	501.28
Ag2				
0.294	0.680	55.74	0.227	974.01
0.490	0.599	49.10	0.200	914.16
0.980	0.415	34.01	0.138	760.82
1.961	0.298	24.43	0.099	644.82
2.942	0.278	22.79	0.093	622.80
Ag3				
0.294	0.787	64.51	0.262	1093.03
0.490	0.703	57.62	0.234	1033.01
0.980	0.438	35.90	0.146	815.39
1.961	0.332	27.21	0.111	709.88
2.942	0.314	25.74	0.105	690.44
Ag4				
0.294	0.894	73.28	0.298	1205.16
0.490	0.797	65.32	0.266	1137.82
0.980	0.515	42.21	0.172	914.66
1.961	0.371	30.41	0.124	776.35
2.942	0.345	28.28	0.115	748.67
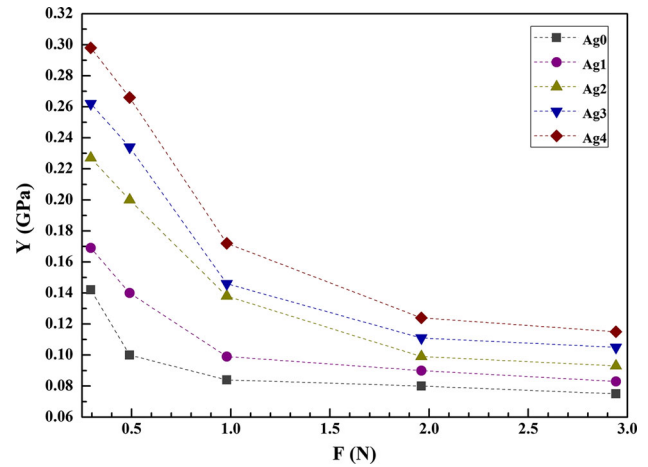
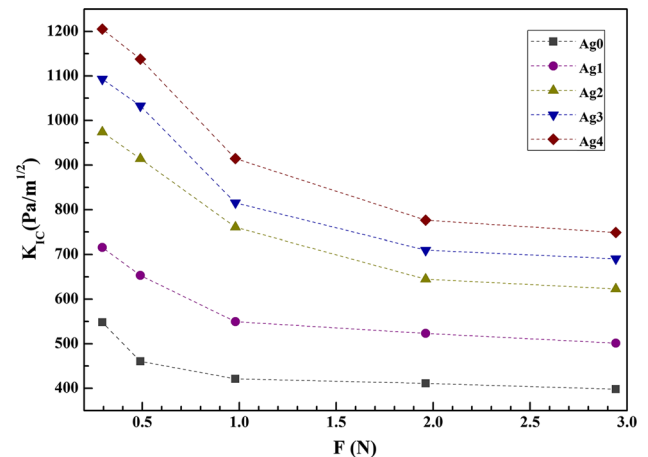**Fig. 5** Variation of yield strength as a function of applied load

Fig. 6 Variation of fracture toughness as a function of applied load

linear regression coefficients are high, this model is not suitable for our results because of the difference between the calculated results and true hardness values.
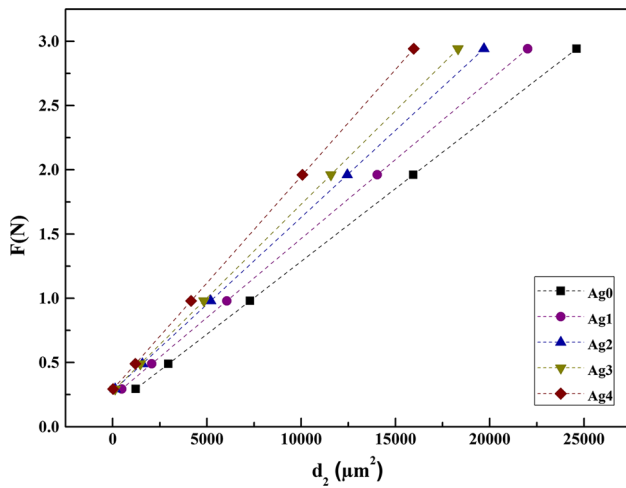
Fig. 7 Graph of the applied load against the square of the diagonal length for the samples

Fig. 8 Plots of diagonal length versus square root of applied loads for the samples

Table 3 Best-fit results of experimental data according to Eq. (7)

Sample	H_o	d_e	LRC	Plateau region H_v (GPa)
Ag0	0.177	−17.34	0.99844	0.239–0.224
Ag1	0.185	−23.01	0.99811	0.270–0.248
Ag2	0.191	−27.70	0.9969	0.298–0.278
Ag3	0.209	−27.00	0.99767	0.332–0.314
Ag4	0.232	−26.07	0.99673	0.371–0.345

Table 4 Best-fit results of experimental data according to energy dissipation model

Sample	H_o	F_o	LRC	Plateau region H_v (GPa)
Ag0	0.210	0.15513	0.99855	0.239–0.224
Ag1	0.228	0.23549	0.9950	0.270–0.248
Ag2	0.251	0.27651	0.99462	0.298–0.278
Ag3	0.270	0.27536	0.99591	0.332–0.314
Ag4	0.308	0.28949	0.99354	0.371–0.345

The second model considers energy dissipative processes during the indentation rather than elastic processes. In this model, a true microhardness can be defined by subtracting a dissipative part, F_0, from the applied load [36].

$$H_0 = 1854.4 \frac{(F - F_0)}{d^2} \quad (Gpa) \qquad (8)$$

Figure 8 shows applied load as a function of the square of the diagonal length for the samples. It is seen from the figure that a good linear relationship is noticed for all the samples. The slope of each line corresponds to the load independent hardness constant, H_0, and the intercept of each line represents the sample resistance pressure, F_0. The extracted values of F_0, H_0 and LRC are deduced by Eq. (8) and are tabulated in Table 4. As can be seen from this table, both the values of F_0 and the values H_0 of the samples increased with increasing Ag doped rates. The extracted load independent microhardness value of Ag substituted sample is closer to the hardness results in the plateau region. The LRC of each sample is very high (R > 0.994). The energy dissipation model also provides a satisfactory description for measured indentation data for samples. We can conclude that the second method is more convenient than the first method for our experimental data.
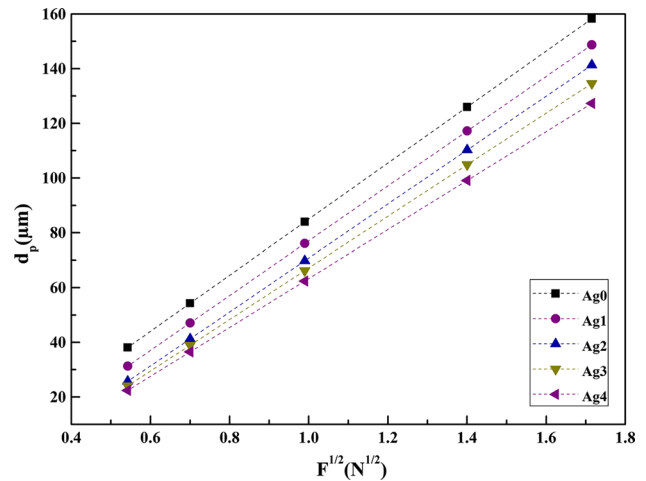
4 Conclusions

The effects of Ag substitution on the structural and mechanical properties of Bi-2223 superconducting system were investigated in this study. Bulk polycrystalline samples with general formula of $Bi_{1.7}Pb_{0.3}Sr_2Ca_2Cu_{3-x}Ag_xO_y$ (x = 0.00, 0.03, 0.06, 0.09, 0.12) were prepared by solid state reaction method. XRD and SEM were used for structural characterization of the samples. Microhardness measurements were performed to determine the mechanical properties of the samples. The indentation load versus diagonal length of the samples under different indentation loads in the range of 0.245–2.940 N were presented. Vickers hardness, Young's modulus, yield strength, fracture toughness values were calculated and these mechanical properties of the samples were found to be load and doping dependent.

According to XRD analysis, increasing the amount of Ag substitution decreases the volume fraction of 2223 phase while increasing volume fraction of 2212 phase. In addition, XRD results showed that lattice parameters a and b did not change when parameter c decreased with Ag doping.

SEM results show that grain size of the samples increase and the surface structure improve by the grain connections

and porosity decreasing with doping Ag. The increase in the microhardness values is associated with the increase in the porosity between the grains. SEM micrographs of all samples with Ag addition show a common feature of plate-like layered grains.

Microhardness measurements were performed to investigate the effects of Ag addition on the mechanical properties of materials which showed Vickers hardness values increase with increasing Ag addition. This can be explained with Ag atoms can settle between particles and into the gaps between the particle surface thus the mechanical characteristics of the samples increases. Vickers microhardness (H_v), elastic modulus (E), yield strength (Y) and fracture toughness (K_{IC}) values decrease with the increase in the applied load. Moreover, ISE behavior is also observed for our samples due to decrease in microhardness values with applied load. In order to understand this behavior, some models such as elastic–plastic deformation model (EPD) and the energy dissipative model were used and it was found that energy dissipative model is suitable for describing the experimental data.

References

1. S. Safran, A. Kılıç, E. Kılıçarslan, H. Ozturk, M. Alp, E. Asikuzun, O. Ozturk, J. Supercond. Nov. Magn. **26**, 3215–3219 (2013)
2. M. Musa, Abbas. Int. J. Curr. Eng. Technol. **5**, 1908–1913 (2015)
3. U. Kölemen, O. Uzun, C. Emeksiz, F. Yılmaz, A. Coşkun, A. Ekicibil, B. Özçelik, J. Supercond. Nov. Magn. **26**, 3215–3219 (2013)
4. B. Özkurt, J. Supercond. Nov. Magn. **26**, 261–266 (2013)
5. G. Yildirim, S. Bal, E. Yucel, M. Dogruer, M. Akdogan, A. Varilci, C. Terzioglu, J. Supercond. Nov. Magn. **25**, 381–390 (2012)
6. A. Saoudel, A. Amira, Y. Boudjadja, L. Amirouche, N. Mahamdioua, A. Varilci, S.P. Altintas, C. Terzioglu, J. Supercond. Nov. Magn. **26**, 861–865 (2013)
7. M. Erdem, Ö. Öztürk, E. Yucel, S.P. Altintas, A. Varilci, C. Terzioğlu, I. Belenli, Phys. B **406**, 705–709 (2011)
8. N.G. Margiani, I.R. Metskhvarishvili, N.A. Papunashvili, D.I. Dzanashvili, G.A. Shurgaia, J. Supercond. Nov. Magn. **24**, 2275–2278 (2011)
9. I. Karaca, O. Uzun, U. Kölemen, F. Yılmaz, O. Şahin, J. Alloys Compd. **476**, 486–491 (2009)
10. S.M. Khalil, J. Low Temp. Phys. **143**, 31–44 (2006)
11. S.M. Khalil, J. Phys. Chem. Solids **62**, 457–466 (2001)
12. S.M. Khalil, Phys. B **391**, 130–135 (2007)
13. O. Uzun, U. Kölemen, S. Çelebi, N. Güçlü, J. Eur. Ceram. Soc. **25**, 969–977 (2005)
14. H. Sözeri, N. Ghazanfari, H. Özkan, A. Kilic, Supercond. Sci. Technol. **20**, 522–528 (2007)
15. S. Sakiroğlu, K. Kocabas, J. Supercond. Nov. Magn. **24**, 1321–1325 (2011)
16. A. Sedky, J. Phys. Chem. Solids **70**, 483–488 (2009)
17. M.M. Ibrahim, S.M. Khalil, A.M. Ahmed, J. Phys. Chem. Solids **61**, 1553–1560 (2000)
18. M. Yilmazlar, H.A. Cetinkara, M. Nursoy, O. Ozturk, C. Terzioglu, Phys. C **442**, 101–107 (2006)
19. O. Ozturk, C. Terzioglu, I. Belenli, J. Supercond. Nov. Magn. **24**, 381–390 (2011)
20. S. Salib, M. Mironova, C. Vipulanandan, K. Salama, Supercond. Sci. Technol. **9**, 1071–1076 (1996)
21. S.M. Khalil, Smart Mater. Struct. **14**, 804–810 (2005)
22. Y. Yoshino, A. Iwabuchi, K. Noto, N. Sakai, M. Murakami, Phys. C **357–360**, 796–798 (2001)
23. S.M. Khalil, A.M. Ahmed, Phys. C **452**, 21–28 (2007)
24. O. Bilgili, Y. Selamet, K. Kocabas, J. Supercond. Nov. Magn. **21**, 439–449 (2008)
25. S.M. Hosseinpour-Mashkani, M. Ramezani, A. Sobhani-Nasab, M. Esmaeili-Zare, J. Mater. Sci.: Mater. Electron. **26**, 6086–6091 (2015)
26. S.M. Hosseinpour-Mashkani, M. Maddahfar, A. Sobhani-Nasab, J. Electron. Mater. **45**, 3612 (2016)
27. S.M. Hosseinpour-mashkani, A. Sobhani-Nasab, M. Mehrzad, J. Mater. Sci.: Mater. Electron. **27**, 5758–5763 (2016)
28. A. Sedky, Phys. C **468**, 1041–1046 (2008)
29. C. Terzioğlu, J. Alloys Compd. **509**, 87–93 (2011)
30. H. Aydin, O. Cakiroglu, M. Nursoy, C. Terzioglu, Chin. J. Phys. **47**, 2 (2009)
31. M. Nursoy, M. Yılmazlar, C. Terzioğlu, I. Belenli, J. Alloys Compd. **459**, 399–406 (2008)
32. O. Ozturk, H.A. Cetinkara, E. Asikuzun, M. Akdogan, M. Yilmazlar, C. Terzioglu, J. Mater. Sci.: Mater. Electron. **22**, 1501–1508 (2011)
33. O. Ozturk, E. Asikuzun, M. Erdem, G. Yildirim, O. Yildiz, C. Terzioglu, J. Mater. Sci.: Mater. Electron. **24**, 230–238 (2013)
34. U. Kölemen, O. Uzun, M. Yılmazlar, N. Güçlü, E. Yanmaz, J. Alloys Compd. **415**, 300–306 (2006)
35. M. Yilmazlar, O. Ozturk, O. Gorur, I. Belenli, C. Terzioglu, Supercond. Sci. Technol. **20**, 365–371 (2007)
36. E. Asikuzun, O. Ozturk, H.A. Cetinkara, G. Yildirim, A. Varilci, M. Yılmazlar, C. Terzioglu, J. Mater. Sci.: Mater. Electron. **23**, 1001–1010 (2012)